GA–A22487

PHYSICS OF TURBULENCE CONTROL AND TRANSPORT BARRIER FORMATION IN DIII–D

by
E.J. DOYLE, K.H. BURRELL, T.N. CARLSTROM, S. CODA, J.C. DeBOO, R.D. DURST, R.J. FONCK, P. GOHIL, C.M. GREENFIELD, R.J. GROEBNER, J. KIM, K.W. KIM, R.J. La HAYE, L.L. LAO, E.A. LAZARUS, R.A. MOYER, G. NAVRATIL, T.H. OSBORNE, W.A. PEEBLES, C.L. RETTIG, T.L. RHODES, B.W. RICE, D.P. SCHISSEL, G.M. STAEBLER, E.J. STRAIT, T.S. TAYLOR, D.M. THOMAS, and R.E. WALTZ

OCTOBER 1996

GA–A22487

PHYSICS OF TURBULENCE CONTROL AND TRANSPORT BARRIER FORMATION IN DIII–D

by

E.J. DOYLE,* K.H. BURRELL, T.N. CARLSTROM, S. CODA,† J.C. DeBOO, R.D. DURST,‡ R.J. FONCK,‡ P. GOHIL, C.M. GREENFIELD, R.J. GROEBNER, J. KIM, K.W. KIM,* R.J. La HAYE, L.L. LAO, E.A. LAZARUS,△ R.A. MOYER,§ G. NAVRATIL,# T.H. OSBORNE, W.A. PEEBLES,* C.L. RETTIG,* T.L. RHODES,* B.W. RICE,◊ D.P. SCHISSEL, G.M. STAEBLER, E.J. STRAIT, T.S. TAYLOR, D.M. THOMAS, and R.E. WALTZ

This is a preprint of a paper to be presented at the 16th IAEA International Conference on Plasma Physics and Controlled Nuclear Fusion Research, October 7–11, 1996, Montreal, Canada and to be published in the *Proceedings.*

***University of California, Los Angeles, California.**
†Massachusetts Institute of Technology, Cambridge, Massachusetts.
‡University of Wisconsin, Madison, Wisconsin.
△Oak Ridge National Laboratory, Oak Ridge, Tennessee.
§University of California, San Diego, California.
#Columbia University, New York, New York.
◊Lawrence Livermore National Laboratory, Livermore, California.

**Work supported by
the U.S. Department of Energy
under Grant and Contract Nos. DE-AC03-89ER51114, DE-FG03-86ER53225, DE-FG02-91ER54109, DE-FG02-92ER54139, DE-AC05-96OR22464, DE-FG03-95ER54294, DE-FG02-89ER53297, W-7405-ENG-48**

**GA PROJECT 3466
OCTOBER 1996**

DISCLAIMER

F1-CN-64/A6-4

PHYSICS OF TURBULENCE CONTROL AND TRANSPORT BARRIER FORMATION IN DIII–D

ABSTRACT

This paper describes the physical mechanisms responsible for turbulence control and transport barrier formation on DIII–D as determined from a synthesis of results from different enhanced confinement regimes, including quantitative and qualitative comparisons to theory. A wide range of DIII–D data support the hypothesis that a *single underlying physical mechanism, turbulence suppression via* ***E×B*** *shear flow* is playing an essential, though not necessarily unique, role in reducing turbulence and transport in all of the following improved confinement regimes: H–mode, VH–mode, high-ℓ_i modes, improved performance counter-injection L–mode discharges and high performance negative central shear (NCS) discharges. DIII–D data also indicate that synergistic effects are important in some cases, as in NCS discharges where negative magnetic shear also plays a role in transport barrier formation. This work indicates that in order to control turbulence and transport it is important to focus on understanding physical mechanisms, such as **E×B** shear, *which can regulate and control entire classes of turbulent modes*, and thus control transport. In the highest performance DIII–D discharges, NCS plasmas with a VH–mode like edge, turbulence is suppressed at *all* radii, resulting in neoclassical levels of ion transport over most of the plasma volume.

1. INTRODUCTION

Improved understanding and control of cross-field transport have long been primary objectives of the magnetic fusion research program — improved/controlled transport characteristics are essential for economical power plant operation. Over the years, a number of improved confinement regimes have been discovered each of which has distinct operational limits and characteristics. However, results from studies of turbulence and transport behavior in improved transport regimes on DIII–D indicate that a single underlying physical mechanism, turbulence suppression via **E×B** shear flow [1,2] is playing an essential, though not necessarily unique, role in reducing turbulence and transport in all of the following improved confinement regimes: H–mode, VH–mode, high-ℓ_i modes, improved performance counter-injection L–mode discharges and high performance negative central shear (NCS) discharges. From these results several conclusions can be drawn: (1) **E×B** shear decorrelation of turbulence and transport provides a unifying physical explanation for the improved transport observed in a wide range of confinement regimes. (2) Shear suppression of turbulence is a robust mechanism, with a demonstrated ability to control turbulence and transport at all radii. (3) Identification of the individual modes responsible for the observed turbulence is not as important as knowledge of turbulence drive and suppression mechanisms, which can provide a direct route to transport control.

E×B shear suppression of turbulence in a plasma is a mechanism akin to the interaction between sheared velocity fields and turbulence in fluids. In a plasma, however, the fundamental velocity is not the mass velocity, but rather the **E×B** velocity, the velocity at which turbulent eddies are convected [3]. Theoretically, shear (first deriva-

tive) in the **E**×**B** velocity can decorrelate turbulence, resulting in decreased radial correlation lengths and a significant reduction in turbulence and transport [4,5]. Fluctuation suppression is predicted to occur when the shearing rate associated with the **E**×**B** flow, $\omega_{\mathbf{E}\times\mathbf{B}}$ exceeds the decorrelation rate of the ambient turbulence $\Delta\omega_T$ [4]. An alternate criterion for turbulence stabilization can also be utilized: numerical simulations suggest that turbulence should be quenched if the shearing rate $\omega_{\mathbf{E}\times\mathbf{B}}$ equals or exceeds the linear growth rate γ of the most unstable mode present [6,7]. Other theoretical predictions are that **E**×**B** shear is a general mechanism which can control the saturation level of entire classes of turbulent modes [8], and that for some modes the curvature (second spatial derivative) of the **E**×**B** velocity can be important [9]. On DIII–D, reductions in turbulence levels, and decreased transport have been observed in all cases where the **E**×**B** shear is large enough to be theoretically significant.

E×**B** shear as a control mechanism for turbulence and transport has the major advantage of flexibility, in that the shear can be generated or enhanced in several different ways. The radial electric field E_r is determined from the lowest order radial force balance equation for a single ion species,

$$E_r = (Z_i e n_i)^{-1} \nabla P_i - v_{\theta i} B_\varphi + v_{\varphi i} B_\theta, \tag{1}$$

where i labels the ion species, Z_i is the charge of the ion, n_i the ion density, e is the electronic charge, P_i the ion pressure, $v_{\theta i}$ and $v_{\varphi i}$ are the ion poloidal and toroidal rotation velocities, and B_θ and B_φ are the poloidal and toroidal magnetic fields, respectively. In general toroidal geometry, it has recently been shown that the shearing rate $\omega_{\mathbf{E}\times\mathbf{B}}$ depends on E_r/RB_θ [10], explicitly

$$\omega_{\mathbf{E}\times\mathbf{B}} = \left| \left[(RB_\theta)^2/B\right] \partial/\partial\Psi (E_r/RB_\theta) \right|, \tag{2}$$

where Ψ is the radial flux coordinate. The significance of this latter result is that E_r/RB_θ behaves quite differently than the magnitude of the **E**×**B** velocity, E_r/B_φ, and is susceptible to modification by changing both E_r and the current profile distribution, which changes B_θ. Note that $\omega_{\mathbf{E}\times\mathbf{B}}$ is not a constant on a flux surface; the $(RB_\theta)^2/B$ term results in different shearing rates on the low and high field sides of a flux surface in a tokamak. Thus, E_r and **E**×**B** shear can be created and/or modified by poloidal and toroidal flows, pressure gradients, and by varying the current profile so as to modify B_θ.

The results presented in this paper have been obtained from a synthesis of results from a sustained multi-year program to investigate the turbulence and transport characteristics of enhanced confinement regimes on DIII–D. Emphasis has been placed on studying the physics of initial transport barrier formation as a high leverage route to understanding the underlying physical mechanisms responsible for the improved transport and confinement. A summary of the results from the different enhanced confinement regimes is given below, followed by conclusions drawn from the entire data set. Note that in this paper the term “transport barrier” is used in a generalized sense — in the highest performance DIII–D discharges, for example, transport is improved across the entire plasma radius.

2. EDGE L–H TRANSITION DATA

The edge region provides the largest data set for this study, and also the most advanced quantitative comparisons to theory. Early measurements in fast transitions

(D_α drop time <1 ms) [11–15] and dithering transitions [16] demonstrated a spatial and temporal correlation between the creation of a region of sheared **E**×**B** flow inside the separatrix, suppression of turbulence levels, and improved transport. Shown in Fig. 1 are more recent Langmuir probe data showing the sheared edge E_r well created inside the separatrix in an Ohmic H–mode, and also showing the resulting change in density and potential fluctuation levels across the transition [shown as a ratio of H–mode (H) to Ohmic (L) levels] [17]. As can be seen, density fluctuations are reduced at all radii shown by a factor of up to 10, while potential fluctuations are reduced everywhere except at the bottom of the E_r well structure, where the shear is approximately zero.

By operating close to the power threshold it has been possible to generate slow L–H transitions (D_α drop time a few ms), in which the time evolution of the edge parameters is sufficiently slow to demonstrate a sequence of events consistent with a causal role for E_r [17–19]. In Fig. 2, floating potential data from the Langmuir probe are shown from 5 mm inside the separatrix and at the separatrix radius. At a time 6 ms before the transition, the floating potentials are similar at the two radii, indicating that E_r is small. However, the difference between the dc floating potentials is observed to change ~4 ms *before* the transition, indicating an increase in the magnitude of E_r. At the transition, the dc potentials change more rapidly, while the fluctuating component of the floating potential signal is suppressed within 30–60 μs. Thus, the initial change in these plasmas occurs in E_r, followed by turbulence suppression, consistent with causality. As the fluctuations are unchanged during the period of the initial change in E_r, these results also indicate that there is a threshold shear level required to suppress turbulence.

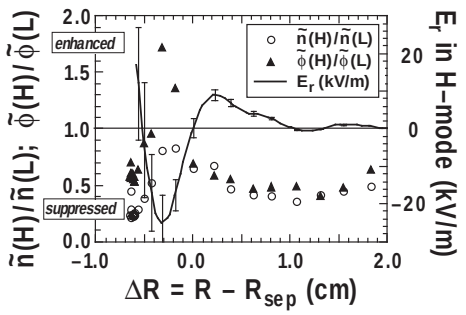

Fig. 1. Radial profile of the radial electric field E_r (solid line) and the ratios of the absolute RMS density and potential fluctuation levels in the H–mode (H) to the values in the Ohmic (L) phase. The density fluctuation data are represented by circles, and the potential by triangles.

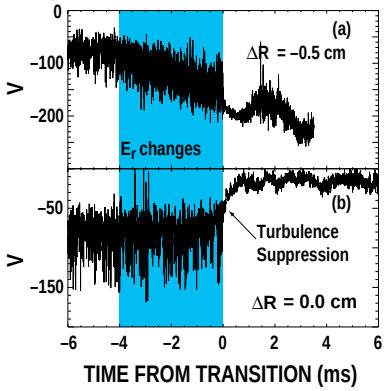

Fig. 2. Time evolution of the floating potential φ_f across an L–H transition at locations (a) 0.5 cm inside the separatrix, and (b) at the separatrix. The potential values begin to change ~ 4 ms before the transition, consistent with a causal role for E_r.

Several quantitative comparisons have also been performed between the experimental results and simple, single fluctuating field theories. Measurements of edge turbulence characteristics across the L–H transition indicate that the edge **E**×**B** shear level generated on the low field side in H–mode is quantitatively more than sufficient to suppress turbulence ($\omega_{\mathbf{E}\times\mathbf{B}} > 5\Delta\omega_T$), as observed [15]. However, a spatial asymmetry in turbulence response is observed; fluctuations on the high field side of DIII–D are not suppressed at the L H transition, consistent with the inboard/outboard variation in the **E**×**B** shearing rate as given by Eq. (2) [14,15]. The spatial profiles

obtained from the Langmuir probe measurements shown in Fig. 1 can also be compared to theoretical predictions for turbulence reduction as a function of shear level [17]. Several models relate the change in relative fluctuation amplitude Θ across the transition to shear levels in the following way:

$$\Theta \equiv \langle \tilde{n}/n \rangle_H / \langle \tilde{n}/n \rangle_L = 1/(a + b|dE_r/dr|^c) , \quad (3)$$

where a and b are parameters that depend upon L–mode turbulence characteristics, and c =2/3 in the high shear model of Biglari, et al., (BDT model) [4], c = 2 in the low shear model of Shaing, et al. [5], and c = 2 in the arbitrary shear model of Zhang and Mahajan [20]. A fit of these models to the data is shown in Fig. 3. As can be seen, the BDT model fits the data well in its range of validity ($|dE_r/dr| > 200$ V/cm^2), while the Zhang and Mahajan model works well at all shears. In the fit of the BDT model, data from regions of positive E_r shear were excluded since the amount of suppression observed differs depending on the sign of the shear (see Fig. 1). In general, the spatial dependence of the edge turbulence reduction is consistent with shear suppression for negative E_r shear, while for positive E_r shear the turbulence suppression is consistent with the effect of E_r shear plus curvature for modes for which an E_r well is destabilizing [17].

However, the experimental data also clearly demonstrate that simple, single field, theories such as [4,5,20] are inadequate to explain all the observed L–H transition phenomena: (1) the response of the density and potential fluctuations to the applied shear clearly differs (Fig. 1), while in the simple models their response should be identical. (2) The cross-phase between the density and potential fluctuations, which is not included in simple theories, plays a very important role in reducing turbulent driven transport in H–mode. For the same data as shown in Fig. 1, the turbulent driven particle flux is substantially reduced in H–mode at all radii, even though potential fluctuations increased in H–mode at some radii. This occurs because the cross-phase changed from $\sim\pi/2$ in Ohmic to $\sim\pi$ in H–mode in the region of least turbulence suppression, reducing the turbulence induced particle flux to ~0, irrespective of fluctuation amplitude. The measured turbulent particle flux on the outboard midplane is large enough to account for the observed edge particle transport rates [21]. (3) Equation 2 contains no threshold for E_r shear effects on turbulence, while experimentally a threshold is observed. (4) The amount of turbulence suppression is observed to depend on the sign of the shear, while theory [Eq. (3)] is independent of sign. (5) The rapidity of the turbulence suppression observed in fast transitions (30–60 μs) [17,18], is inconsistent with the range for the exponent $2/3 < c < 2$, obtained from the spatial profiles described above. For the theoretical models to replicate such fast suppressions requires a much larger exponent, $c \sim 4$ [22]. The conclusion from these five points is that self-consistent theories (theories which account for the response of the turbulence and plasma parameters to the imposed $\mathbf{E}\times\mathbf{B}$ shear) are essential in modeling the L–H transition. Such theories have been developed, e.g., Refs. [9,23], but, predictably, they are much harder to test experimentally.

New aspects of the L–H transition mechanism still exist which require further study. For example, an additional type of "very slow" transition has been observed on DIII–D in which the edge D_α emission can take >50 ms to evolve from L– to H–mode levels. These very slow transitions occur at power levels close to threshold, such that at first they were thought to be possible examples of a slow phase transition. However, recent results indicate that these very slow transitions occur close to threshold in relatively high density plasmas where there is a MARFE and/or divertor detachment in L–mode. In H–mode, the MARFE dissipates. Thus, the time scale for very slow L–H

transitions may be governed by the time scale of the atomic physics processes involved in MARFE burn-through. Another difference between very slow and fast transitions is that in many very slow transition discharges the SOL profiles and turbulence levels remain unchanged from L– mode to the early H–mode phase, i.e., the turbulence suppression occurs only inside the separatrix.

3. VH–MODE DISCHARGES

VH–mode results from an inward expansion of the H–mode transport barrier to smaller major radius [24,25]. Increased confinement is attributed to increased **E**×**B** shear in the outer core region, due to an increase in core toroidal rotation rates – an example of a core transport bifurcation based on **E**×**B** decorrelation of turbulence as discussed in [26]. Illustrated in Fig. 4 are the changes in the **E**×**B** shearing rate $\omega_{\mathbf{E}\times\mathbf{B}}$ and effective thermal diffusivity χ_{eff} between the H– and VH–mode phases of a single discharge. As shown by the shaded regions, the shearing rate is substantially larger in VH–mode, with a marked decrease in transport in the same region. Shown in Fig. 4(a) by the horizontal line and inscription "BDT EDGE" is an estimate of the shearing rate predicted by the BDT model [4] to suppress edge turbulence, based on DIII–D L–mode edge turbulence data [17]. In VH–mode, the region where the shearing rate exceeds the level required for edge turbulence suppression expands inward to $\rho \sim 0.6$. Coincident with the increase in **E**×**B** shear, turbulence is reduced. Shown in Fig. 5, are time histories of the density fluctuations level at $\rho \sim 0.8$, and toroidal rotation velocities at several locations during the H– and VH–mode phases of a single discharge. The increased shear associated with VH–mode operation is shown directly by the divergence at ~2360 ms of the toroidal rotation traces a radial location of at $\rho \sim 0.8$. Density fluctuation levels at $\rho \sim 0.8$ decrease by a factor of ~2 in VH–mode compared with the H–mode phase, and short regular bursts in the fluctuation level disappear. These bursts

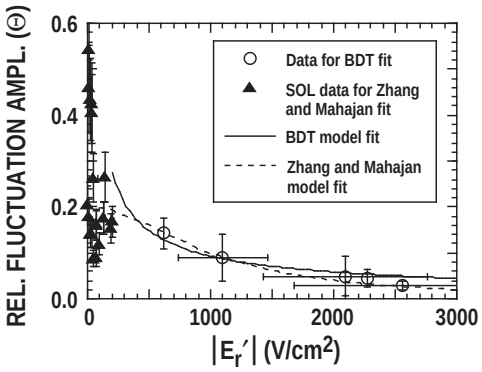

Fig. 3. Experimentally observed dependence of the relative fluctuation amplitude Θ on the magnitude of the E_r shear. The lines represent fits to theory, showing quantitative agreement.

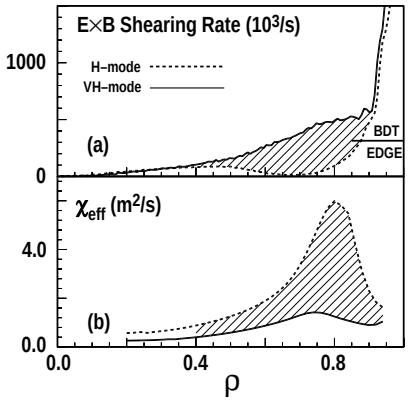

Fig. 4. Changes in the radial profiles of (a) the **E x B** shearing rate ω_{ExB}, and (b) effective thermal diffusivity χ_{eff} from the H– to the VH–mode phase of a single discharge. The dashed lines are H–mode, solid lines VH–mode. Also marked in Fig. 4(a) by the horizontal line and inscription "BDT EDGE" is an estimate of the shearing rate required to suppress edge turbulence based on DIII–D L–mode turbulence data.

of turbulence are associated with changes in the toroidal rotation profile in the same region, leading to the term "momentum transfer events" (MTEs) [25]. The repetitive nature of the fluctuation bursts associated with MTEs is similar to the limit-cycle behavior predicted for core turbulence in Ref. [27]. More complete details of the turbulence reduction observed in VH–mode have been published in Refs. [3,25,28]. Finally, magnetic braking experiments in VH–mode discharges have demonstrated a clear causal role for **E**×**B** shear in reducing turbulence and transport [3,28,29]. Similar magnetic braking experiments are described in more detail in the next section.

4. HIGH-ℓ_i DISCHARGES

In high-ℓ_i discharges, the plasma elongation is rapidly increased, thereby increasing the internal inductance ℓ_i and peaking B_θ [30]. The transport improvement observed in high-ℓ_i discharges is attributed to the modified current profile increasing the shear in E_r/RB_θ, resulting in increased toroidal rotation and consequent turbulence suppression. Magnetic braking of toroidal rotation in high-ℓ_i discharges reduces the **E**×**B** shearing rate, leading to an increase in turbulence and transport [31]. These braking experiments provide a direct demonstration that **E**×**B** shear plays a *causal role* in the reduced turbulence and transport normally observed in these plasmas. Shown in Fig. 6 are comparisons of the shearing rate $\omega_{\mathbf{E}\times\mathbf{B}}$ and single fluid χ_{eff} with and without magnetic braking in high-ℓ_i discharges. As shown by the shaded regions in Fig. 5, the application of the magnetic brake reduces the **E**×**B** shearing rate, resulting in a substantial increase in transport. Coincident with the application of the magnetic brake and increase in transport, fluctuation levels as monitored by the FIR scattering system increase by a factor of ~2–3. Turning off the brake allows the plasma rotation and confinement to return to unbraked levels.

5. COUNTER-INJECTION L–MODE DATA

Results from DIII–D [32] indicate that **E**×**B** shear suppression of turbulent fluctuations may also play a causal role in the improved confinement observed in

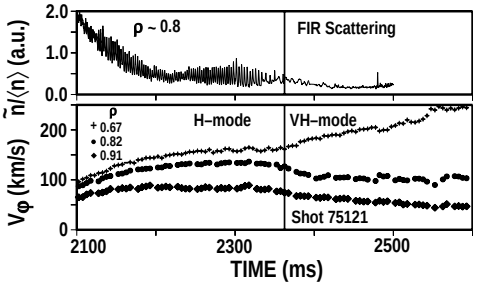

Fig. 5. Time evolution of density fluctuation levels, as monitored by an FIR scattering system, and impurity ion toroidal rotation velocities at several radial locations during the evolution of a single discharge from H–mode to VH–mode.

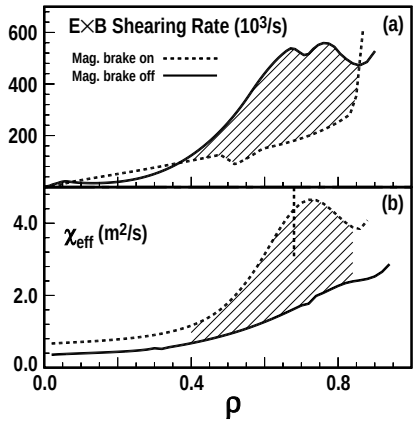

Fig. 6. Comparisons of (a) the **ExB** shearing rate ω_{ExB}, and (b) single fluid χ_{eff} radial profiles with and without magnetic braking in separate high-ℓ_i discharges. The dashed lines are with magnetic braking, solid lines without.

counter-injection L–mode plasmas on several machines [33,34]. On DIII–D, counter-injection leads to significant changes in E_r as compared with Ohmic or co-injection plasmas. E_r in Ohmic discharges is typically positive across the entire plasma radius. Application of counter neutral injection changes both the magnitude and polarity of E_r, since E_r in the core is dominated by the toroidal rotation term in Eq. 1. Fluctuation data obtained during these discharges indicate a two-step turbulence response after the initiation of counter injection. First is a prompt (within 5–10 ms) reduction of about 30% in fluctuation levels for fluctuations with wavenumbers greater than approximately 2 cm^{-1}. On a longer time scale, the overall fluctuation level integrated over all wavenumbers decreases further by another factor of ~30%. That the changes in E_r and **E**×**B** shear consequent upon the initiation of counter injection are responsible for this reduction in turbulence levels is strongly suggested by the time coincidence of the observations and also by the lack of changes in other relevant profile parameters during this time.

6. NEGATIVE CENTRAL SHEAR (NCS) DISCHARGES

There are several reasons to believe that **E**×**B** shear effects are playing an essential role in controlling turbulence and transport in high performance NCS discharges [35–39]: (a) large central gradients in the toroidal rotation profile, combined with the modified current profile distribution, generate significant levels of **E**×**B** shear in the core of NCS discharges. Shown in Fig. 7 is a comparison of E_r and **E**×**B** shearing rate profiles for an NCS plasma with an L–mode edge and a VH–mode discharge. The shearing rate is clearly higher in the core of the NCS plasma, while the VH–mode plasma has a superior shearing rate in the outer half of the plasma. After transport barrier formation in NCS plasmas the **E**×**B** shearing rate clearly exceeds the trapped electron η_i mode linear growth rate in the region of reduced transport, whereas the two rates are comparable immediately before barrier formation [36], i.e., $\omega_{\mathbf{E}\times\mathbf{B}}$ is quantitatively large enough to suppress turbulence such as η_i modes and, hence, reduce transport. (b) NCS is not necessary for the maintenance of high performance; performance is maintained in discharges where the current profile evolves such that the core magnetic shear becomes low or slightly positive [36]. However, high levels of **E**×**B** shear are maintained. (c) Negative magnetic shear is predicted to locally lower the threshold for turbulence suppression via **E**×**B** shear, further facilitating **E**×**B** shear suppression of turbulence in NCS discharges [40]. (d) A power threshold has to be exceeded before turbulence and transport are reduced, in agreement with **E**×**B** shear theory [26,40,41]. While this threshold seems to be sharp on TFTR [42], DIII–D data indicate a more gradual improvement in transport with increasing power.

In addition to **E**×**B** shear, negative magnetic shear also contributes to the formation of high performance NCS discharges. NCS enhances plasma stability and suppresses ballooning modes [35,43] and may also stabilize drift-type microinstabilities [44,45]. Thus, DIII–D data support a picture in which the enhanced performance in the NCS regime is obtained via a combination of *both magnetic and **E**×**B** shear effects*. As a result, very low levels of turbulence and transport are observed in NCS discharges; BES measurements indicate $\tilde{n}/n$ levels of <0.1% in the core of NCS with an L–mode edge, as compared to 0.5-1.0% in conventional L–mode plasmas. The width of this core transport barrier region expands from the center outwards with additional power and collapses from the outside in when power is reduced. This latter observation is in accord with theoretical predictions, which typically contain a local transport bifurcation which is a function of local power density [26,40,41].

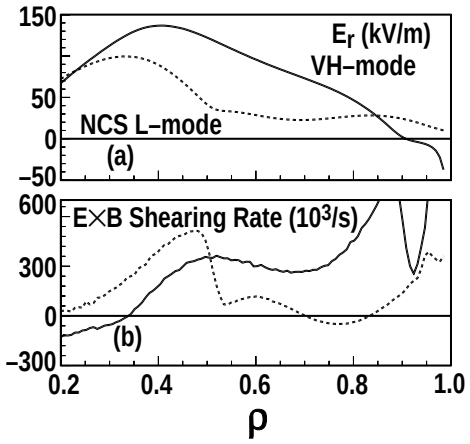

Fig. 7. Comparisons of (a) E_r profiles, and (b) the **ExB** shearing rate ω_{ExB}, in NCS (L–mode edge) and VH–mode plasmas. The dashed lines are NCS data. Solid lines VH–mode.

By inducing an edge L–H transition, the highest performance DIII–D NCS discharges combine the core turbulence suppression obtained in NCS discharges with an L–mode edge, with the edge turbulence suppression of VH–mode discharges, resulting in turbulence suppression at *all* radii. An example of the time evolution of the density fluctuations as determined by FIR scattering in the highest performance DIII–D discharge (87977) is shown as a color coded contour plot in Fig. 8, with an additional plot showing the evolution of the neutron rate. While the inherent spatial resolution of the FIR scattering system is poor, the spatial variation of the **E**×**B** induced Doppler shifts, which dominate the scattered signal, allow us to associate frequency with position. Thus, large positive frequencies are associated with the plasma core on the low field side, frequencies close to zero correspond to the plasma edge and the magnetic axis, while large negative frequencies correspond to the plasma core on the high field side. Using this frequency/spatial mapping, Fig. 8 can be interpreted as follows: At the start of the high power beam phase at 2160 ms core turbulence is convected at increasing velocity (frequency) as plasma rotation increases. At the same time, the core fluctuation level decreases until it is entirely suppressed by 2300 ms. At 2300 ms the plasma edge transitions from L– to H–mode, and edge turbulence is rapidly suppressed. From 2400 to 2600 ms, *broadband density turbulence is suppressed across the entire plasma radius* during which period the neutron rate rises rapidly. At 2560 ms, coherent MHD is observed, leading to a slowing in the rate of increase of the neutron rate. The peak plasma neutron rate occurs at 2630 ms, coinciding with a return of broadband turbulence. As shown in Fig. 9, the high performance phase of this discharge achieved neoclassical levels of ion transport over most of the plasma volume [38,39]. This achievement of neoclassical ion transport and turbulence suppression across most of the plasma volume fulfills a longstanding goal of the magnetic confinement fusion research program.

Other significant observations in NCS plasmas include the following: A core transport barrier is often observed to form gradually in the initial low-power heating phase, before the main heating beams are applied. As shown in Fig. 8, the residual turbulence in high performance NCS plasma often exhibit a regular bursting character in time, reminiscent of the limit-cycle behavior predicted in Ref. [27] and of the

turbulence bursts associated with MTEs in VH–mode. A spatial asymmetry in the turbulence suppression is also observed on occasion during periods in which the **E**×**B** shear is decreasing. As the shear decreases, turbulence and/or MHD are observed to increase preferentially on the high field side which, like the spatial asymmetry observed in the edge at the L–H transition, is thought to originate in the non-equal shearing rates on the high and low field sides, see Section 2 above. Finally, one remaining puzzle in these discharges is that the improvement in electron transport is much less dramatic than that in other channels [36,39].

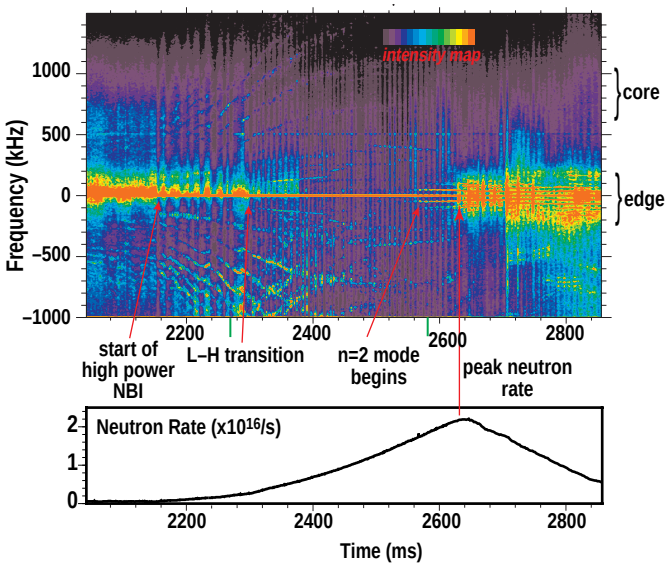

Fig. 8. Color contour plot of time evolution of density fluctuations in the highest performance DIII–D NCS discharge. Data are from FIR scattering system at a wavenumber of 2 cm^{-1}. Darker colors correspond to lower fluctuation levels (black lowest), brighter to higher (red highest). Also shown is the evolution of the neutron rate.

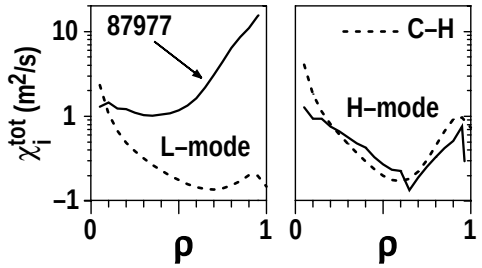

Fig. 9. Ion thermal diffusivity versus ρ for the same discharge as shown in Fig. 8. (a) L–mode phase at 2275 ms, and (b) H–mode at 2580 ms. The solid lines are the experimental values, the dashed lines calculated neoclassical values using the Chang-Hinton formula [46].

7. CONCLUSIONS AND SUMMARY

A synthesis of results from DIII–D indicates that sheared **E**×**B** flow is playing an essential role in the formation and maintenance of a wide range of transport barriers and reduced transport regimes. The evidence for this conclusion can be summarized under the following headings: *1. Causality*. Edge measurements at the L–H transition provide evidence for a causal role for **E**×**B** shear, as do magnetic braking experiments in VH– and high-ℓ_i modes. *2. Quantitative tests of theory*. Edge turbulence measurements across the L–H transition show quantitative agreement with theory. The observed **E**×**B** shearing rates in all regimes are of sufficient magnitude that turbulence reduction can be expected. 3*. Qualitative tests of theory*. Measurements in all reduced transport regimes indicate a spatial and temporal correlation between the development of **E**×**B** shear and reduced turbulence and transport. Other processes, such as magnetic shear effects are also important and can operate in parallel in a synergistic fashion. From these results, several conclusions can be drawn: (a) **E**×**B** shear regulation of turbulence and transport provides a unifying physical basis for the improved transport observed in a wide range of confinement regimes (b) Shear suppression of turbulence is a robust mechanism, with a demonstrated ability to control turbulence and transport at all radii. (c) Identification of the individual modes responsible for the observed turbulence may not be as important as knowledge of turbulence drive and suppression mechanisms, which can provide a direct route to transport control. By combining the turbulence suppression features of NCS and VH–mode plasmas, the highest performance DIII–D discharges exhibit turbulence suppression at *all* radii, resulting in neoclassical levels of ion transport over most of the plasma volume [38,39].

ACKNOWLEDGMENTS

This is a report of work supported by the U.S. Department of Energy under Grant and Contract Nos. DE-AC03-89ER51114, DE-FG03-86ER53225, DE-FG03-95ER54294, DE-AC05-96OR22464, W-7405-ENG-48, DE-FG02-91ER54109, DE-FG02-92ER54139, and DE-FG02-89ER53297.

REFERENCES

[1] GROEBNER, R.J., Phys. Fluids B **5**, 2343 (1993).
[2] ITOH, K, ITOH, S.-I., Plasma Phys. Control. Fusion **38**, 1 (1996).
[3] BURRELL, K.H., et al., Phys. Plasmas **1**, 1536 (1994).
[4] BIGLARI, H., et al., Phys. Fluids B **2**, 1 (1990).
[5] SHAING, K.C, et al., Phys. Fluids B **2**, 1492 (1990).
[6] WALTZ, R.E., et al., Phys. Plasma **1**, 2229 (1994).
[7] WALTZ, R.E., et al., Phys. Plasma **2**, 2408 (1995).
[8] HASSAM, A.B., Comments Plasma Phys. Controlled Fusion **14**, 275 (1991).
[9] CARRERAS, B.A., et al., Phys. Fluids B **5**, 1491 (1993).
[10] HAMN, T.S., BURRELL, K.H., Phys. Plasmas **2**, 1648 (1995).
[11] GROEBNER, R.J., et al., Phys. Rev. Lett. **64**, 3015 (1990).
[12] BURRELL, K.H., et al., Phys. Fluids B **2**, 1405 (1990).
[13] DOYLE, E..J., et al., Phys. Fluids B **3**, 2300 (1991).
[14] BURRELL, K.H., et al., Plasma Phys. Control. Fusion **34**, 1859 (1992).

[15] DOYLE, E..J., et al., Plasma Physics and Controlled Nuclear Fusion Research 1992 (IAEA, Vienna, 1993), Vol. 1, 235.
[16] MATSUMOTO, H., et al., Plasma Phys. Control. Fusion **34**, 615 (1992).
[17] MOYER, R.A., et al., Phys. Plasmas **2**, 2397 (1995).
[18] BURRELL, K.H., et al., Plasma Physics and Controlled Nuclear Fusion Research 1994 (IAEA, Vienna, 1995), Vol. 1, 221.
[19] GROEBNER, R.J., et al., AIP Conference Proceedings 345, International Conf. on Plasma Physics ICPP 1994, AIP Press, New York (1995) 74-82.
[20] ZHANG, Y.Z., MAHAJAN, S.M., Phys. Fluids B **4**, 1385 (1992).
[21] MOYER, R.A., et al., to be published in J. Nuc. Mater. (1996).
[22] STAEBLER, G.M., et al., Bull. American Phys. Soc. **39**, 1616, 4P26 (1994).
[23] DIAMOND, P.H., et al., Phys. Rev. Lett. **72**, 2565 (1994).
[24] JACKSON, G.L. et al., Phys. Rev. Lett. **67**, 3098 (1991).
[25] OSBORNE, T.H., et al., Nucl. Fusion **35**, 23 (1995).
[26] STAEBLER, G.M., et al., Phys. Plasmas **1**, 909 (1994).
[27] CARRERAS, B.A., et al., Phys. Plasma **2** , 2744 (1995).
[28] RETTIG, C.L., et al., Plasma Phys. Control. Fusion **36**, A207 (1994).
[29] LA HAYE, R.J., et al., Nucl. Fusion **35**, 988 (1995).
[30] LAO. L.L., et al., Phys. Rev. Lett. **70**, 3435 (1993).
[31] LA HAYE, R.J., et al., in Local Transport Studies in Fusion Plasmas, J.D. CALLEN et al., editors, Bologna (1993) 283.
[32] RETTIG, C.L., et al., Phys. Plasmas **3**, 2374 (1996).
[33] GEHRE, O., et al., Phys. Rev. Lett. **60**, 1502 (1988).
[34] IDA, K., , et al., Phys. Rev. Lett. **68**, 182 (1992).
[35] STRAIT, E.J., et al., Phys. Rev. Lett. **75**, 4421 (1995).
[36] LAO, L.L., et al., Phys. Plasma **3**, 1951 (1996).
[37] RICE, B.W., et al., Phys. Plasma **3**, 1983 (1996).
[38] LAZARUS, E.A., et al., Phys. Rev. Lett, **77**, 2714 (1996), and Paper F1-CN-64/A1-2 these Proceedings.
[39] SCHISSEL, D.P., et al., Paper F1-CN-64/A5-3, these Proceedings.
[40] DIAMOND, P.H., et al., submitted to Phys. Rev. Lett. (1996).
[41] DIAMOND, P.H., et al.,Phys. Plasmas **2**, 3685 (1995).
[42] LEVINTON, F.M., et al., Phys. Rev. Lett. **75**, 4417 (1995).
[43] TURNBULL, A.D., et al., Phys. Rev. Lett. **74**, 718 (1995).
[44] KADMOMSEV, B.B, POGUTSE, O.P., Sov. Phys. JETP **24**, 1172 (1967).
[45] KESSEL, C., et al., Phys. Rev. Lett. **72**, 1212 (1994).
[46] CHANG, C.S., HINTON, F.L., Phys Fluids **29**, 3314 (1986).